# Developing a Kinematically Similar Master Device for Extensible Continuum Robot Manipulators

**Chase G. Frazelle**[1]
Mechatronics Laboratory,
Department of Electrical and Computer Engineering,
Clemson University,
Clemson, SC 29630
e-mail: cfrazel@clemson.edu

**Apoorva Kapadia**
Department of Electrical and Computer Engineering,
Clemson University,
Clemson, SC 29630
e-mail: akapadi@clemson.edu

**Ian Walker**
Department of Electrical and Computer Engineering,
Clemson University,
Clemson, SC 29630
e-mail: iwalker@clemson.edu

*We introduce a novel input device for the teleoperation of extensible continuum robots. As opposed to previous works limited by kinematically dissimilar master devices or restricted degrees-of-freedom (DoF), a kinematically similar input device capable of 9DoF is designed and used. The device is capable of achieving configurations identical to a three-section continuum robot and simplifies the teleoperation of such manipulators. In this paper, we outline the design of the input device and its construction. Implementation of the new master device and its effectiveness in regulating a physical system is also discussed.*
[DOI: 10.1115/1.4039075]

## 1 Introduction

Teleoperation continues to be an area of robotics that is necessary for the development and testing of robotic systems. The ability to interact with a remote environment through a robotic system remains a major advantage when dealing with hazardous situations and unstable surroundings [1]. Despite extensive research in the topic of teleoperation [2], the subject is still open to innovation, especially when concerning less conventional continuum robots.

Continuum robots [3] present a unique control problem due to their unusual structure. Unlike rigid-link robots that feature a discrete set of joints capable of rotating or extending at fixed points, continuum robots are capable of bending at any point along their backbone. Developed from the biological inspiration of animal kingdom structures (tentacles, tongues, and elephant trunks), continuum robots are able to perform a unique range of environmental interactions in comparison to traditional manipulators [4,5]. Continuum robots have exhibited numerous system designs and applications in a variety of environments [6–11].

Extensive research has been conducted into the kinematic modeling of continuum robots [12,13]. Research has also led to approximations of Jacobian models [14] and more exact models such as Refs. [15–17]. These Jacobians allow for responsive real-time implementation of continuum manipulators. Further advances have been made in the research of the customary control of continuum robots including dynamics [18–21] and control [22–26]. The topics of dynamics and control are still active areas of research in continuum robotics. While much attention has been given to these aspects of continuum manipulator operation, the human interfacing and teleoperation of continuum robots has only seen a handful of investigations in the literature [6]. One limiting factor on the teleoperation of continuum robots has been the lack of intuitive relationships between a human interface and a continuum system.

In the literature, there are three examples of teleoperation schemes concerning continuum manipulators. In Ref. [27], the movements of a traditional gaming joystick are mapped to the motions of a continuum robot. A series of mappings were created and tested. Though the system was functional, the limited degrees-of-freedom (DoF) of gaming joysticks (two or three degrees-of-freedom) created difficulties in translating the movements of the joystick to the movements of the manipulator. In Ref. [28], a nonredundant rigid-link master was used to manipulate the end effector of a planar continuum robot. This system did not directly manipulate the 6DoF available to the planar continuum manipulator, instead using the inverse Jacobian to determine the necessary input values for the end effector to reach a desired point. Though this application is useful, it does not take into account the environment of the manipulator and cannot be used in applications such as whole arm manipulation [15]. A third recent study used of a 6DoF rigid-link robot to teleoperate both the planar and spatial motion of a 9DoF continuum robot [29]. In this study, several mappings were developed to directly control the 9DoF of the continuum robot. The system allowed users to manipulate the slave manipulator and perform various tasks but still lacked fully intuitive teleoperation of the continuum robot, especially in regard to the location of the end effector. All of these investigations demonstrated useful capabilities in the teleoperation of continuum robots but each had shortcomings in various aspects, especially concerning intuitive interfacing.

In this paper, we present a teleoperation input device designed for intuitive continuum manipulator interfacing. The continuum input device, nicknamed the MiniOct, is a three-section continuum device capable of extending and curving each of its three sections. With the additional ability to curve in any direction, the device is capable of kinematically emulating a 9DoF continuum manipulator. We demonstrate the use of the MiniOct to teleoperate two 9DoF continuum robots and discuss the versatility of the input device. The results indicate that the MiniOct device is a significant advance in the direction of intuitive continuum manipulator interfacing. This work is an extension of the work presented in Ref. [30].

The paper is organized in the following order: Section 2 describes the design inspiration and construction of the MiniOct, as well as details about the materials and hardware utilized. Section 3 reviews a demonstration of the device being used to teleoperate two different continuum manipulators in real time. Discussion and conclusions are made in Secs. 4 and 5, respectively.

## 2 Design and Construction

The MiniOct is a three-section continuum device that is capable of kinematically emulating a three-section, 9DoF continuum slave device. The mechanical design of the device was inspired by the spring and cable system present in the elephant trunk manipulator [31]. The total system measures 71.59 cm in height and weighs approximately 1.57 kg. The device is comprised of two main hardware components: the continuum input interface and the configuration measurement system. The two components can be seen in Fig. 1, where section A is the continuum input interface and section B is the measurement system.

[1]Corresponding author.

Contributed by the Mechanisms and Robotics Committee of ASME for publication in the JOURNAL OF MECHANISMS AND ROBOTICS. Manuscript received September 22, 2017; final manuscript received January 17, 2018; published online February 5, 2018. Editor: Venkat Krovi.

  

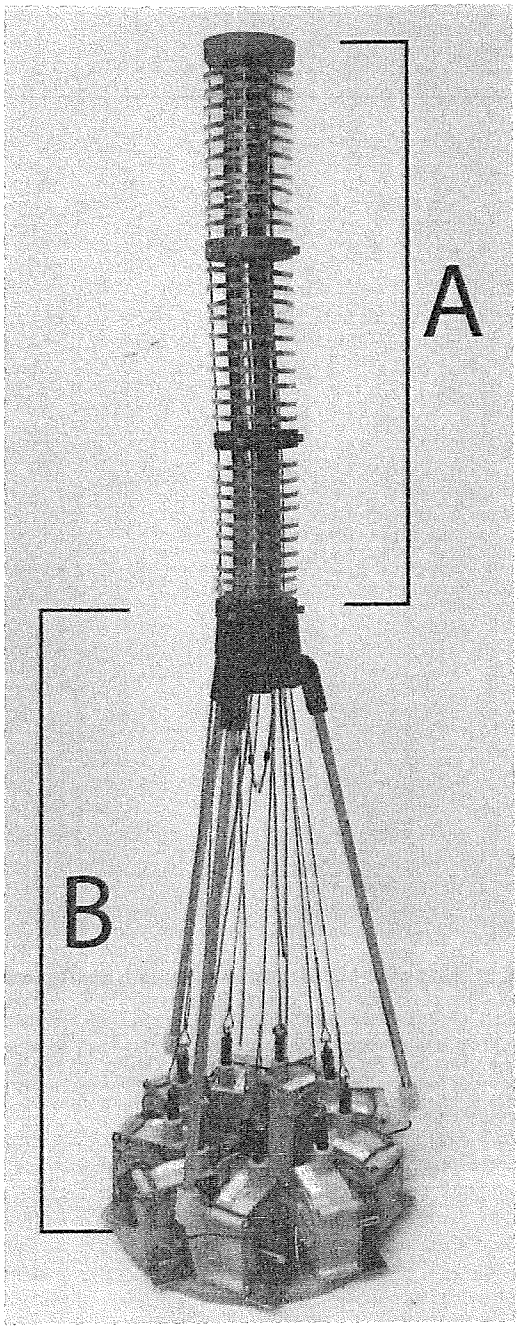


Fig. 1 MiniOct continuum input device

**2.1 Continuum Interface.** Similarly to Ref. [31], a parallel system of cables and springs allow the MiniOct to curve and extend with constant curvature for each of the three sections. Unlike the elephant trunk manipulator [31], the MiniOct only uses three springs and three cables per section, similar to the actuation of the OctArm manipulator [32] it is designed to teleoperate. Additionally, the MiniOct is constructed with extension springs, whereas the elephant trunk used compression springs. The use of extension springs in the MiniOct design creates a default configuration in which the MiniOct is at the minimum length and contains no curve along the length of the device. The length of the entire continuum interface section ranges from 31.75 cm to 57.16 cm. This change in length is constrained by the string potentiometers described in Sec. 2.2, which have a maximum extension of 30.48 cm.

The springs used within each section were chosen to have low spring constant and an unextended length of approximately 10 cm.

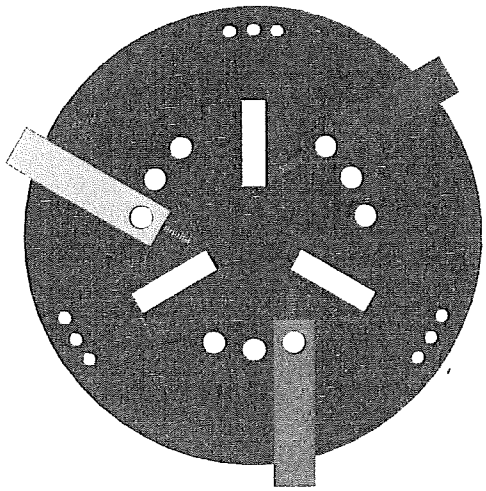

Fig. 2 Cross section of push tab system

This choice in spring length allows each section to nearly double in length and a lower spring constant reduces the resistance to extension experienced by the user. The outer diameter of the springs chosen to meet these criteria was 0.95 cm. A system of cables within each section use friction to maintain any configuration achieved from manipulation by a user.

The friction imposed on each cable is created by placing spring loaded tabs at the base of each section. These tabs encircle the cables and press against them to prevent slipping in either direction. When pressed by a user, the tabs allow the cable to glide freely, extending or compressing the side of the immediately distal section to which the tab corresponds. A cross section of a section divider with the tabs for each cable can be seen in Fig. 2.

The section dividers are three-dimensional printed cylinders designed to be rotationally symmetric at intervals of 120 deg with slots for the termination of section springs, holes for each cable, and internal tracks for the cable tabs. The section dividers are assigned different colors to help distinguish the sections for the operator. Also featured in each divider is a series of smaller holes that allow for the passage of thin cables attached to the measurement devices that determine the configuration of the MiniOct. These devices are described in Sec. 2.2. The diameter of the section dividers, and the overall device, was set at 5.08 cm in order to accommodate the springs, cables, and push tabs.

In order to create constant curvature, each section is fitted with a series of acrylic spacers that keep the relative distance between the springs and cables constant. These spacers prevent the buckling of the springs and force each section to curve in a desirable fashion, creating constant curvature for the cables. They are fixed at equal intervals along the extension springs using transparent cord. An example of a spacer for the base section can be seen in Fig. 3. Each section contains ten acrylic spacers.

A cross-sectional view of a single MiniOct section is seen in Fig. 4. The operation of a section is described by the arrows, in which the operator first presses the push tab and then extends the structural cables by pulling on the end of the section. Releasing the tabs causes the section to hold the set configuration. When pressing the push tabs without the operator holding the end of the section, the springs will retract the support cables to the default section length.

**2.2 Configuration Measurement.** In order to use the MiniOct as a master device in the teleoperation of continuum manipulators, the device must be able to output information that can be used to determine the configuration of the device and thus the desired configuration of the slave device. For the MiniOct, this information is provided in the form of nine cable length measurements, three lengths for each section placed 120 deg apart. These

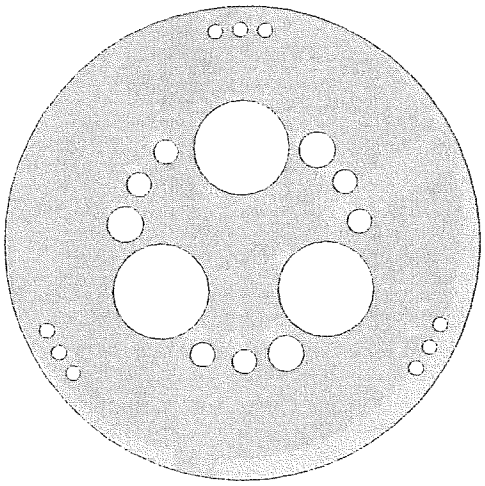

Fig. 3 Acrylic spacer for base section of MiniOct

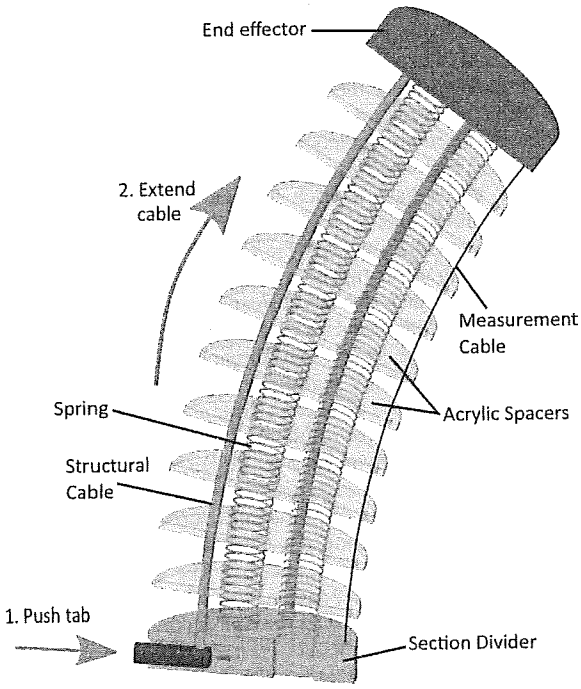


Fig. 4 Basic operation of single MiniOct section

measurements are read as voltages, ranging from 0 V to 5 V, from a series of string potentiometers, which are placed symmetrically in a circle at the base of the device. The circle of potentiometers can be seen in Fig. 5.

The string potentiometers in use are voltage dividers that increase output signal in direct proportion to the length in which the string is extended. Each of the potentiometers is attached to a cable running along the length of the MiniOct and terminating at the end of the base, middle, or tip section. The output voltages are then converted to useable values using the following equations:

$$\ell_{bi} = (V_{bi})\frac{\Delta_{\ell b}}{V_{\max}} + \ell_{b\min} \tag{1}$$

$$\ell_{mi} = (V_{mi} - V_{bi})\frac{\Delta_{\ell m}}{V_{\max}} + \ell_{m\min} \tag{2}$$

$$\ell_{ti} = (V_{ti} - V_{mi})\frac{\Delta_{\ell t}}{V_{\max}} + \ell_{t\min} \tag{3}$$

Fig. 5 Ring of string pots for determining configuration

where $\ell_{bi}$, $\ell_{mi}$, and $\ell_{ti}$ are the calculated output (desired for the slave device) lengths for the base, middle, and tip sections, respectively, of the slave device for the $i$th actuator in each section. $Vb_i$, $V_{mi}$, and $V_{ti}$ are the output voltages from the MiniOct string pots, again corresponding to the base, middle, and tip sections for the $i$th string pot for each section. $\Delta_{lb}$, $\Delta_{lm}$, and $\Delta_{lt}$ are the total change in length achievable by each section of the slave device and $\ell_{b\min}$, $\ell_{m\min}$, and $\ell_{t\min}$ are the minimum section lengths of the slave device. $V_{\max}$ is the maximum voltage that can be output from the MiniOct by fully extending a single section. The values of $\ell_{bi}$, $\ell_{mi}$, and $\ell_{ti}$ can be used to calculate meaningful values for the kinematics of a slave device or can be directly used to calculate slave device input such as pneumatic pressure or tendon length.

## 3 System Implementation

Following the development of the hardware and signal output, the device was utilized for the teleoperation of two structurally different continuum manipulators. The two slave manipulators were the OctArm [32] and the Tendril [33] manipulators. The setup for these two devices is described in Secs. 3.1 and 3.2, respectively.

**3.1 MiniOct to OctArm.** The OctArm is pneumatically driven by a series of pressure regulators controlled via a Quanser data acquisition board [34]. The input values for the regulators are derived in a SIMULINK model [35]. In this experiment, the output lengths from the MiniOct were obtained using the Quanser board and converted to OctArm section lengths within the same SIMULINK model used to manipulate the OctArm. Once converted to lengths

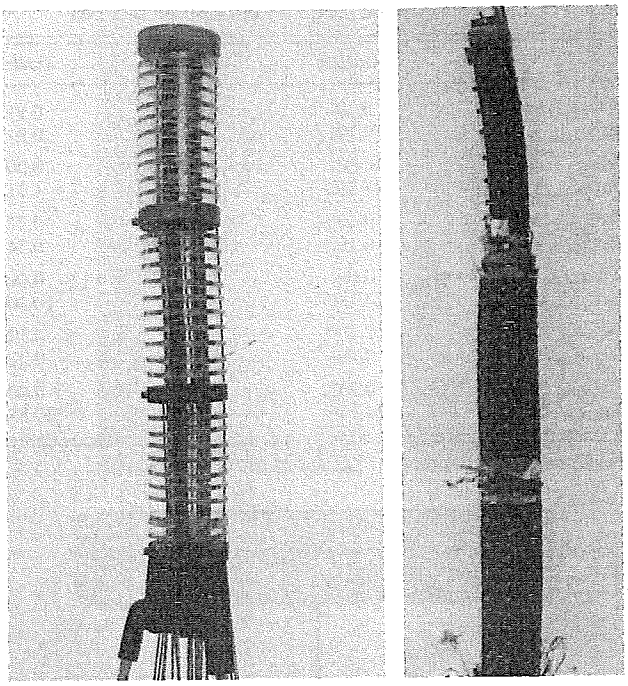

**Fig. 6 Correlation of base, middle, and tip sections**

using Eqs. (1)–(3), the values are used to calculate the necessary pressures to achieve the configuration designated by the MiniOct.

In order to increase the intuitiveness of the MiniOct's design, the device is color coded to allow a user to easily determine the relative orientation between the master and slave devices. In this experiment, the OctArm was similarly marked with blue, green, and red tapes to indicate which of the base, middle, and tip sections, respectively, was curving in response to the MiniOct configuration. Additional color labeling was used to determine orientation of the bending sections by corresponding to the colors of the push tabs on the master device. Figure 6 depicts the base, middle, and tip sections of the MiniOct and OctArm, where both devices are oriented such that the base sections are located near the bottom of the image and the tip sections are located near the top of the image. In order to demonstrate the functionality of the MiniOct, a series of configurations were reached that show the relationship between the MiniOct and the OctArm. These teleoperation experiments directly mapped MiniOct cable lengths to OctArm muscle lengths using open-loop control. Figures 7(*a*) and 7(*b*) demonstrate curving of a single section with two differing orientations. The first orientation is toward the view of the user while the second is perpendicular to the view. Figure 7(*c*) shows the actuation of the middle section while keeping the base and tip sections without curve or extension. Figure 7(*d*) is an example of curving two sections, each with a different orientation. The final configuration, seen in Fig. 8, shows manipulation of all three of the OctArm sections using the MiniOct.

As can be seen in Fig. 7, the orientation of the slave device mirrors that of the MiniOct. In these experiments, this relationship between orientations was created for the clarity of the results. The motion of the slave device can be changed to occur in the same coordinate frame as the MiniOct or in a mirrored coordinate frame. Figure 7(*a*) highlights the respective coordinate frames between the two devices, where the MiniOct is operating in a right-hand coordinate frame and the OctArm operates in a left-hand coordinate frame. The axes shown depict the $X$, $Y$, and $Z$ axes as arrows traveling right to left, out from the image, and from the bottom to the top of the image, respectively.

The physical range for the MiniOct, OctArm, and Tendril with respect to curvature and arc length can be seen in Table 1. The table also highlights the significant differences between the two slave systems demonstrated in these experiments. The range for direction of curvature is the same for all three devices, given that all three are capable of curving each section in any direction.

**3.2 MiniOct to Tendril.** The Tendril manipulator differs structurally and operationally from the OctArm, creating another potential application for the MiniOct. As opposed to pneumatic actuation and a similar range of length for each section of the OctArm, the Tendril is tendon actuated and each of the three sections has a unique range of backbone length. The default lengths of the three Tendril sections at rest are approximately 90 cm, 35 cm, and 20 cm for the base, middle, and tip sections, respectively, as seen in Table 1. In order to implement the MiniOct as a master device for the Tendril, the kinematic values arc length, curvature, and angle of curvature (denoted $s$, $\kappa$, and $\phi$ as described in Ref. [16]) were used to map the shape of the MiniOct to the shape

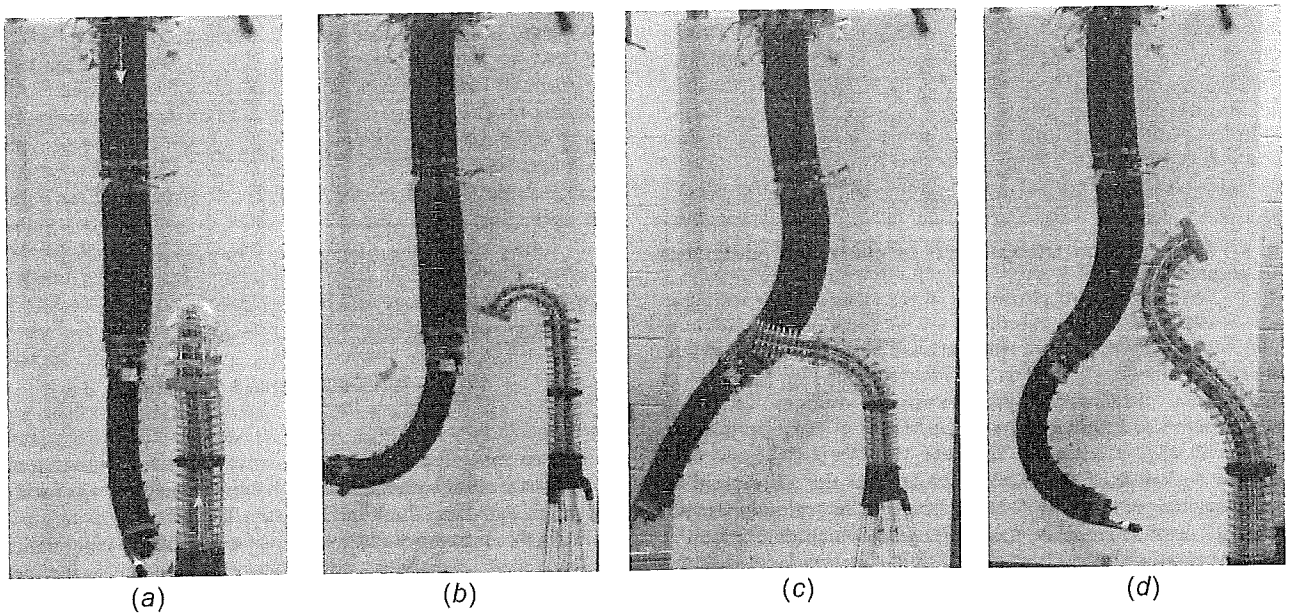


**Fig. 7 Configurations between MiniOct and OctArm manipulator with local coordinate frames: (*a*) curving tip section (i), (*b*) curving tip section (ii), (*c*) curving middle section, and (*d*) two section manipulation**

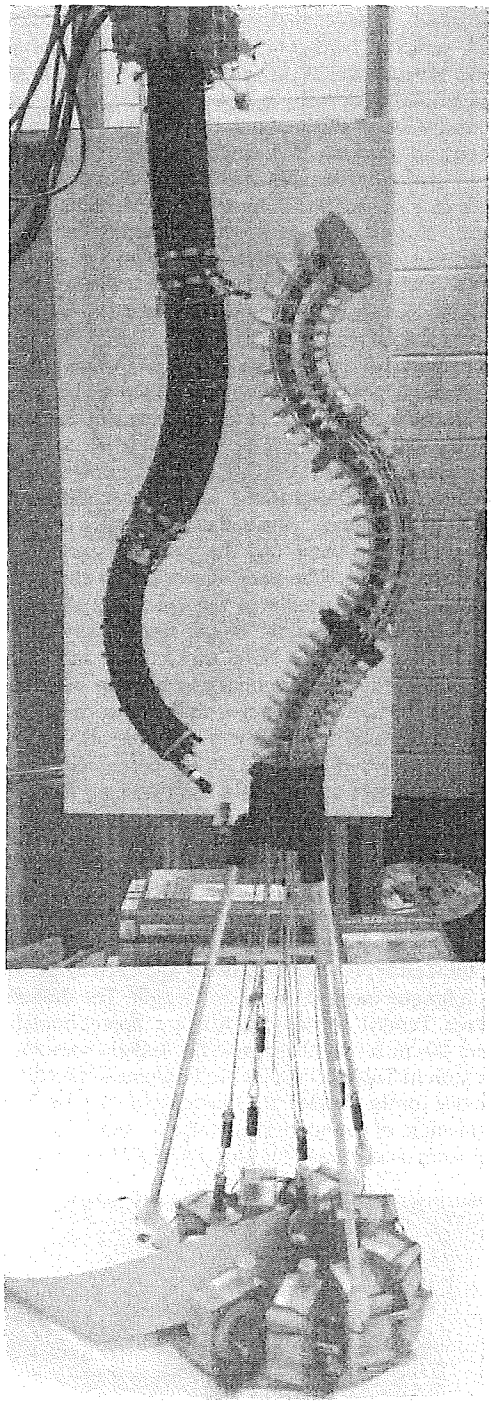

**Fig. 8 Three section teleoperation of pneumatic continuum manipulator**

of the Tendril. The procedure for mapping MiniOct lengths to tendon lengths for the Tendril is demonstrated in Fig. 9. MiniOct lengths are again calculated by converting the voltages from string potentiometers to actual lengths of the MiniOct. These lengths are used to calculate $s$, $\kappa$, and $\phi$ for each MiniOct section and then scaled to the range of $s$, $\kappa$, and $\phi$ available to the corresponding Tendril section as listed in Table 1. Finally, the scaled kinematic values are used to calculate tendon lengths, which determine the degree of rotation for each of the Tendril's motors located at the base of the manipulator.

In the MiniOct to OctArm experiment, the MiniOct is tethered to the same computer as the OctArm through the Quanser data acquisition board and SIMULINK. The Tendril is designed as a

**Table 1 Kinematic range for continuum devices**

| | MiniOct | OctArm | Tendril |
|---|---|---|---|
| Min $s_{\text{Base}}$ (m) | 0.100 | 0.3233 | 0.917 |
| Max $s_{\text{Base}}$ (m) | 0.180 | 0.418 | 0.917 |
| Min $\kappa_{\text{Base}}$ ($\text{m}^{-1}$) | 0.001 | 0.001 | 0.001 |
| Max $\kappa_{\text{Base}}$ ($\text{m}^{-1}$) | 24.166 | 4.200 | 1.713 |
| Min $s_{\text{Mid}}$ (m) | 0.100 | 0.314 | 0.225 |
| Max $s_{\text{Mid}}$ (m) | 0.180 | 0.418 | 0.345 |
| Min $\kappa_{\text{Mid}}$ ($\text{m}^{-1}$) | 0.001 | 0.001 | 0.001 |
| Max $\kappa_{\text{Mid}}$ ($\text{m}^{-1}$) | 24.166 | 4.450 | 10.300 |
| Min $s_{\text{Tip}}$ (m) | 0.100 | 0.3387 | 0.105 |
| Max $s_{\text{Tip}}$ (m) | 0.180 | 0.455 | 0.215 |
| Min $\kappa_{\text{Tip}}$ ($\text{m}^{-1}$) | 0.001 | 0.001 | 0.001 |
| Max $\kappa_{\text{Tip}}$ ($\text{m}^{-1}$) | 24.166 | 6.000 | 27.557 |

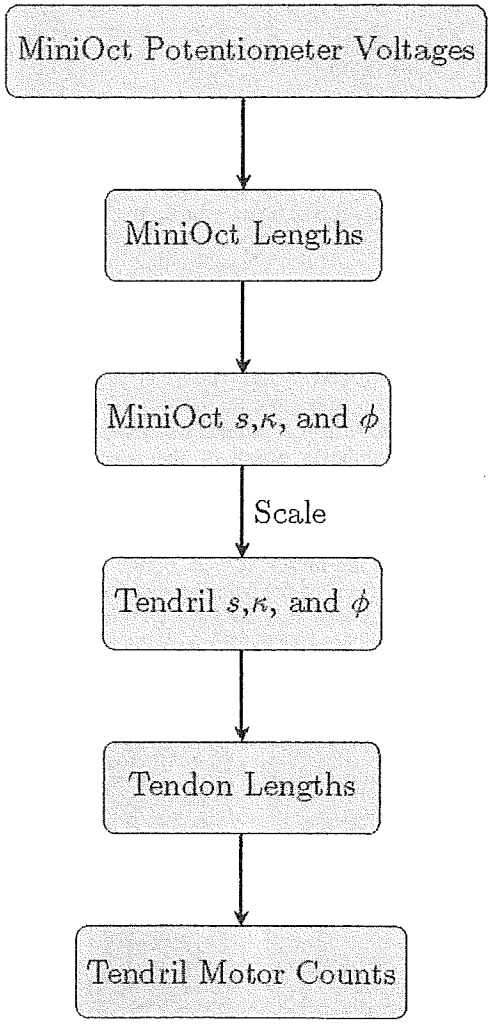


**Fig. 9 MiniOct to Tendril mapping**

mobile system for use in inspection, which calls for a more portable communication system. Bluetooth communication was used to send motor data from the MiniOct to the Tendril.

Bluetooth communication is established via serial communication from an Arduino Mega microcontroller mounted to the measurement section of the MiniOct. The Bluetooth communication is set up such that the MiniOct Bluetooth receiver is the master and the Tendril Bluetooth receiver is set as a slave device that can only connect to the MiniOct receiver. All kinematic calculations

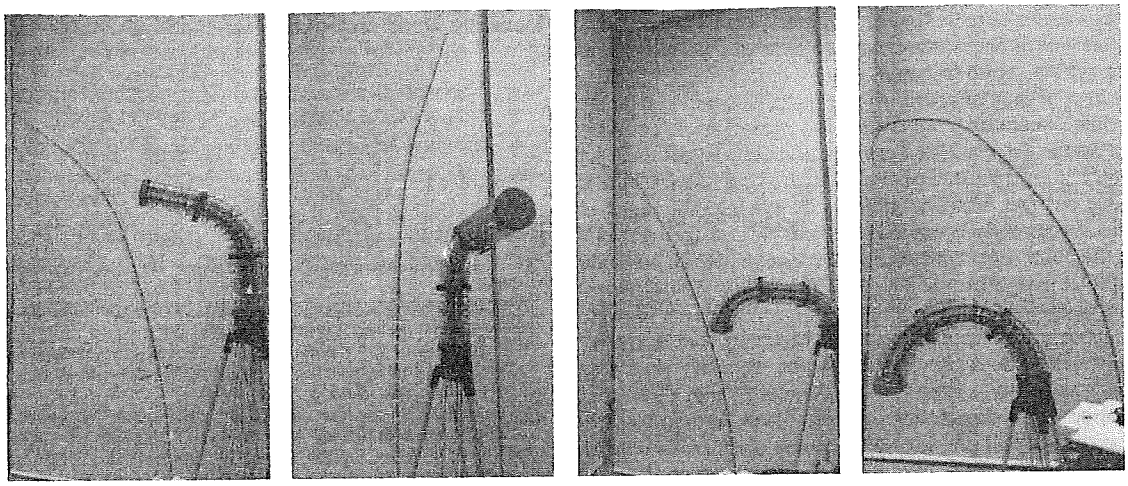


**Fig. 10 Configurations between MiniOct and Tendril manipulator with local coordinate frames: (*a*) curving middle section (i), (*b*) curving middle section (ii), (*c*) curving base and middle section, and (*d*) three section manipulation**

take place in the MiniOct's microcontroller, and motor movement is executed by a microcontroller mounted to the Tendril's motor package.

Similar to the OctArm experimental results, a series of images can be seen in Fig. 10 that showcase the mapping between the MiniOct and the Tendril, which are placed in the same base orientation for these experiments. The orientation between the coordinate frames for the two devices is demonstrated in Fig. 10(*a*), using the same axis description used in Fig. 7(*a*). Figures 10(*a*) and 10(*b*) demonstrate curving of the middle section with differing directions of curvature. Figure 10(*a*) shows both systems curving in the plane perpendicular to the camera and Fig. 10(*b*) depicts the systems curving toward the camera. Figure 10(*c*) demonstrates the mapping from the MiniOct base and tip sections to the Tendril base and tip sections, which have a two different scaling factors given the differences in length. Figure 10(*d*) is an example of mapping to all three sections of the Tendril using the MiniOct.

## 4 Discussion

The goal of this work was to create a small, easy-to-use continuum device capable of acting as a master device for a 9DoF continuum manipulator. The device needed to manipulate extending and curving of three continuum sections in any direction. As seen in Sec. 3, the implementation of the MiniOct controller proved to be simple and very effective. Once constructed, the MiniOct operator was able to intuitively provide direct interfacing to two different 9DoF continuum manipulators with minimal calibration.

There are several critical parameters present in the design of this device. The overall length and change in length is constrained by the use of string potentiometers, which have a maximum extension of 30.48 cm. Given a three section device and a desire to potentially double each section length at full extension, this means that each section could have a default length of 10 cm and a maximum additional extension of 10 cm. In order to maximize ease of use, the springs in each section ideally have a low spring constant and an unextended length of approximately 10 cm. The total outer diameter of the extensible section must accommodate the spacing of the springs, 18 cables (nine cables for structural support, nine for string potentiometers), and the push tabs. A larger radial displacement of the string potentiometers increases the impact of length changes, increasing state estimation accuracy, but the outer circumference of the device must be small enough for the operator grab the device and simultaneously press all three push tabs for a section. The current circumference of the MiniOct does not account for the hand size of the average person, which could be an adjustment for future iterations.

Mechanical and measurement coupling is present between the three sections. Given a change in the base section length, the cable routes and the values measured by the string potentiometers for the middle and tip sections are altered. The mechanical coupling is addressed through the flexibility of the extensible elements. Since the cable system runs the entire length of MiniOct, changing the path in a proximal section does not prevent the manipulation of distal sections, as the cables are still free to glide through the section dividers and spacers. Additionally, distal sections are provided with longer excess structural cable for displacement caused by the extension of a proximal section. The measurement coupling is addressed by subtracting the lengths measured in a proximal section from the immediately distal section. This practice is also performed in other continuum manipulators that rely on string lengths for state estimation.

The rotational offset of the measuring cables routed through the MiniOct introduces a small error in estimating the phase of the master device. There is a phase shift of 6.6 deg between the cables attached to the string potentiometers around the middle channel. This offset is minimized by routing the tip section cable through the middle channel and then placing the base and middle sections cables clockwise and counterclockwise to either side, respectively. Thus, when applying Eqs. (1)–(3), the phase error cancels for the distal sections when actuating all three sections. The phase error for the base section can be eliminated with a constant phase offset after calculating the raw lengths.

While the final design provides ideal direct kinematic mapping, there are some limitations of the device to address. The cable system does well at maintaining the configuration set by the user but the friction imposed by the push tabs is not enough to overcome the spring loaded force of the string potentiometers for large extension of the base section. The base section is subject to the compression force of the three springs within its section and all nine of the string potentiometers, producing more force on the section. The middle and tip sections are able to hold their shape regardless of the extension length. In order to address this problem, the friction on the base cables needs to be increased. Two potential solutions are to increase the surface area of the contact with the push tabs or to use string potentiometers with reduced spring tension.

Additionally, the current design has all elements of the MiniOct exposed to the user. This creates a potential pinch hazard and increases the chance of damage to the device. While the open

design makes repair simple, there is potential benefit to creating an extensible cover for sections. A cover could be developed using a thin rubber sheath or fabric.

Another area of improvement is to develop a way to extend the MiniOct while maintaining curvature. The operation of the MiniOct allows for the extension and curving of a section, but once set to a curvature, it is difficult to extend along that curve without first straightening out the MiniOct section. Design modifications to achieve this are currently being investigated.

Though there are some hardware issues to address, the potential for the MiniOct is significant. The versatility of the device allows for the teleoperation of any three section continuum device, regardless of length or actuation type. The qualitative nature of the results presented does not demonstrate the physical constraints of the master and slave systems, but a novelty of the MiniOct is its ability to scale the device output to any 9DoF extensible continuum manipulator and provide the user with a physical approximation of the slave system. Despite the differences in physical capabilities seen in Table 1, the kinematic range for the MiniOct can easily be scaled to map to either manipulator. The result of scaling the MiniOct output is a slight disassociation between the exact shape of the MiniOct and the slave device (as can be seen in Figs. 7(*b*) and 10), but the general orientation and shape of the slave device is still provided to the operator.

As noted earlier, no past teleoperation devices for continuum robots have been able to directly teleoperate all DoF of a slave device. The MiniOct is unique in having the ability to manipulate the entire configuration of a continuum system and also intuitively manipulate the position and orientation of the end effector. The volume surrounding the MiniOct can be thought to represent a scaled model of the volume surrounding the slave device, including orientation if both devices are mounted in the same base orientation.

The current hardware design allows for individual section manipulation, which is useful when the specific shape of the slave device is important. A feature that can be implemented in software would be the ability to teleoperate all sections of a slave device using only a single section of the MiniOct, or any variety of mappings between one or more sections of the MiniOct to any combination of sections in the slave manipulator. A mapping between a single section of the MiniOct to all sections of a slave system would result in direct end-effector manipulation, but would constrain the possible configurations for the slave device.

Further versatility of the MiniOct is present in the modularity of the sections. The current design has three distinct sections but additional sections could be added once the issue of friction is addressed in the base section. The MiniOct would then be able to teleoperate beyond the 9DoF currently present.

## 5 Conclusion

The teleoperation of an extensible continuum robot using a novel continuum input device was investigated. A description of the design and construction of the device is provided. Device design allows for easy transportation and enables application to a variety of slave style hardware types. The device was used to teleoperate two nine degree-of-freedom continuum robots in spatial motion, demonstrating the capability of the system. The similarity in kinematics allowed for ease of use and intuitive interfacing for the slave systems. The user is able to relate orientation of master and slave devices using visual cues from color of continuum sections. Future work will look to further improve input device design by addressing friction issues and implementing haptic feedback.


## Acknowledgment

This work was supported in part by the U.S. National Science Foundation in part by NASA and in part by a NASA Space Technology Research Fellowship.

## Funding Data

- National Aeronautics and Space Administration (Contract Nos. 80NSSC17K0173 and NNX12AM01G).
- National Science Foundation (Grant No. IIS-1527165).


## References


[1] Niemeyer, G., Preusche, C., and Hirzinger, G., 2008, *Telerobotics*, Springer, Berlin.

[2] Hokayem, P. F., and Spong, M. W., 2006, "Bilateral Teleoperation: An Historical Survey," Automatica, **42**(12), pp. 2035–2057.

[3] Robinson, G., and Davies, J., 1999, "Continuum Robots—A State of the Art," IEEE International Conference on Robotics and Automation (ICRA), Detroit, MI, May 10–15, pp. 2849–2854.

[4] Webster, R., III, and Jones, B. A., 2010, "Design and Modeling of Constant Curvature Continuum Robots," Int. J. Rob. Res., **29**(13), pp. 1661–1683.

[5] Trivedi, D., Rahn, C., Kier, W., and Walker, I., 2008, "Soft Robotics: Biological Inspiration, State of the Art, and Future Research," Appl. Bionics Biomech., **5**(2), pp. 99–117.

[6] Walker, I., 2013, "Continuous Backbone 'Continuum' Robot Manipulators: A Review," ISRN Rob., **2013**(1), pp. 1–19.

[7] Butler, E., Hammond-Oakley, R., Chawarski, S., Gosline, A., Codd, P., Anor, T., Madsen, J., Dupont, P., and Lock, J., 2012, "Robotic Neuro-Endoscope With Concentric Tube Augmentation," IEEE/RSJ International Conference on Intelligent Robots and Systems (IROS), Vilamoura, Portugal, Oct. 7–12, pp. 2941–2946.

[8] Chen, Y., Liang, J., and Hunter, I., 2014, "Modular Continuum Robotic Endoscope Design and Path Planning," IEEE International Conference on Robotics and Automation (ICRA), Hong Kong, China, May 31–June 7, pp. 5393–5398.

[9] Buckingham, R., 2002, "Snake Arm Robots," Ind. Rob.: Int. J., **29**(3), pp. 242–245.

[10] Monapi, M., Godage, I. S., Vijaykumar, A. M., and Walker, I., 2015, "A Novel Continuum Robotic Cable Aimed at Applications in Space," Adv. Rob., **29**(13), pp. 861–875.

[11] Laschi, C., Mazzolai, B., Mattoli, V., Cianchetti, M., and Dario, P., 2009, "Design of a Biomimetic Robotic Octopus Arm," Bioinspiration Biomimetics, 4(1), p. 015006.

[12] Mahl, T., Hildebrandt, A., and Sawodny, O., 2014, "A Variable Curvature Continuum Kinematics for Kinematic Control of the Bionic Handling Assistant," IEEE Trans. Rob., **30**(4), pp. 935–949.

[13] Jones, B., and Walker, I., 2006, "Kinematics of Multisection Continuum Robots," IEEE Trans. Rob., **22**(1), pp. 43–57.

[14] Mochiyama, H., and Kobayashi, H., 1999, "The Shape Jacobian of a Manipulator With Hyper Degrees of Freedom," IEEE International Conference on Robotics and Automation (ICRA), Detroit, MI, May 10–15, pp. 2837–2842.

[15] Gravagne, I., and Walker, I. D., 2002, "Manipulability, Force, and Compliance Analysis for Planar Continuum Manipulators," IEEE Trans. Rob. Autom., **18**(3), pp. 263–273.

[16] Jones, B., and Walker, I., 2004, "A New Approach to Jacobian Formulation for a Class of Multi-Section Continuum Robots," IEEE International Conference on Robotics and Automation (ICRA), Barcelona, Spain, Apr. 18–22, pp. 3279–3284.

[17] Jones, B. A., McMahan, W., and Walker, I. D., 2004, "Design and Analysis of a Novel Pneumatic Manipulator," IFAC Symposium on Mechatronic Systems, Sydney, Australia, Sept. 6–8, pp. 745–750.

[18] Gallot, G., Ibrahimand, O., and Khalil, W., 2007, "Dynamic Modeling and Simulation of a 3-D Hybrid Structure Eel-Like Robot," IEEE International Conference on Robotics and Automation (ICRA), Rome, Italy, Apr. 10–14, pp. 1486–1491.

[19] Kang, R., Kazakidi, A., Guglielmino, E., Branson, D., Tsakiris, D., Ekaterinaris, J., and Caldwell, D., 2011, "Dynamic Model of a Hyper-Redundant Octopus-Like Manipulator for Underwater Applications," IEEE/RSJ International Conference on Intelligent Robots and Systems (IROS), San Francisco, CA, Sept. 25–30, pp. 4054–4059.

[20] Marchese, A., Tedrake, R., and Rus, D., 2015, "Dynamics and Trajectory Optimization for a Soft Spatial Fluidic Elastomer Manipulator," IEEE International Conference on Robotics and Automation (ICRA), Seattle, WA, May 26–30, pp. 2528–2535.

[21] Tatlicioglu, E., Walker, I., and Dawson, D., 2007, "Dynamic Modeling for Planar Extensible Continuum Robot Manipulators," Int. J. Rob. Autom., **24**(4), pp. 1087–1099.

[22] Conrad, B., and Zinn, M., 2015, "Closed Loop Task Space Control of an Interleaved Continuum Rigid Manipulator," IEEE International Conference on Robotics and Automation (ICRA), Seattle, WA, May 26–30, pp. 1743–1750.

[23] Goldman, R., Bajo, A., and Simaan, N., 2014, "Compliant Motion Control for Multisegment Continuum Robots With Actuation Force Sensing," IEEE Trans. Rob., **30**(4), pp. 890–902.

[24] Kapadia, A., Fry, K., and Walker, I., 2014, "Empirical Investigation of Closed-Loop Control of Extensible Continuum Manipulators," IEEE International Conference on Intelligent Robots and Systems (IROS), Chicago, IL, Sept. 14–18, pp. 329–335.

[25] Sadati, S., Noh, Y., Naghibi, S., and Althoefer, A., 2015, "Stiffness Control of Soft Robotic Manipulators for Minimally Invasive Surgery (MIS) Using Scale Jamming," International Conference on Robotics and Automation (ICIRA), Portsmouth, UK, Aug. 24–27, pp. 141–151.

[26] Yip, M., and Camarillo, D., 2014, "Model-Less Feedback Control of Continuum Manipulators in Constrained Environments," IEEE Trans. Rob., 30(4), pp. 880–888.
[27] Csencsits, M., Jones, B., and McMahan, W., 2005, "User Interfaces for Continuum Robot Arms," IEEE International Conference on Intelligent Robots and Systems, pp. 3011–3018.
[28] Kapadia, A., Walker, I., and Tatlicioglu, E., 2012, "Teleoperation Control of a Redundant Continuum Manipulator Using a Non-Redundant Rigid-Link Master," IEEE International Conference on Intelligent Robots and Systems (IROS), Edmonton, AB, Canada, Aug. 2–6, pp. 3105–3110.
[29] Frazelle, C., Kapadia, A., Fry, K., and Walker, I., 2016, "Teleoperation Mappings From Rigid Link Robots to Their Extensible Continuum Counterparts," IEEE International Conference on Robotics and Automation (IROS), Vilamoura, Portugal, Oct. 7–12, pp. 4093–4100.
[30] Frazelle, C., Kapadia, A., and Walker, I., 2017, "Developing a Kinematically Similar Master Device for Extensible Continuum Robot Manipulators," ASME Paper No. DETC2017-67321.
[31] Hannan, M., and Walker, I., 2003, "Kinematics and the Implementation of an Elephant Trunk Manipulator and Other Continuum Style Robots," J. Rob. Syst., **20**(2), pp. 45–63.
[32] Grissom, M., Chitrakaran, V., Dienno, D., Csencsits, M., Pritts, M., Jones, B., McMahan, W., Dawson, D., Rahn, C., and Walker, I., 2006, "Design and Experimental Testing of the OctArm Soft Robot Manipulator," Proc. SPIE, **6230**, pp. 109–114.
[33] Wooten, M. B., and Walker, I. D., 2015, "A Novel Vine-Like Robot for In-Orbit Inspection," International Conference on Environmental Systems, Bellevue, WA, July 12–16, Paper No. 21.
[34] Quanser, 2015, "Q8-USB Data Acquisition Board," Quanser, Markham, ON, Canada, accessed Jan. 29, 2018, http://www.quanser.com/products/q8-usb
[35] MathWorks, 2016, "Simulation and Model Based Design," The MathWorks Inc., Natick, MA, accessed Jan. 29, 2018, http://www.mathworks.com/products/simulink